

Structures of p38 α Active Mutants Reveal Conformational Changes in L16 Loop that Induce Autophosphorylation and Activation

Ron Diskin^{1,2}, Mario Lebendiker¹, David Engelberg² and Oded Livnah^{1,2*}

¹The Wolfson Centre for Applied Structural Biology
The Hebrew University of Jerusalem, Givat Ram
Jerusalem 91904, Israel

²Department of Biological Chemistry, The Silberman Institute of Life Sciences
The Hebrew University of Jerusalem, Givat Ram
Jerusalem 91904, Israel

p38 mitogen-activated protein (MAP) kinases function in numerous signaling processes and are crucial for normal functions of cells and organisms. Abnormal p38 activity is associated with inflammatory diseases and cancers making the understanding of its activation mechanisms highly important. p38s are commonly activated by phosphorylation, catalyzed by MAP kinase kinases (MKKs). Moreover, it was recently revealed that the p38 α is also activated *via* alternative pathways, which are MKK independent. The structural basis of p38 activation, especially in the alternative pathways, is mostly unknown. This lack of structural data hinders the study of p38's biology as well as the development of novel strategies for p38 inhibition. We have recently discovered and optimized a novel set of intrinsically active p38 mutants whose activities are independent of any upstream activation. The high-resolution crystal structures of the intrinsically active p38 α mutants reveal that local alterations in the L16 loop region promote kinase activation. The L16 loop can be thus regarded as a molecular switch that upon conformational changes promotes activation. We suggest that similar conformational changes in L16 loop also occur in natural activation mechanisms of p38 α in T-cells. Our biochemical studies reveal novel mechanistic insights into the activation process of p38. In this regard, the results indicate that the activation mechanism of the mutants involves dimerization and subsequent *trans* autophosphorylation on Thr180 (on the phosphorylation lip). Finally, we suggest a model of *in vivo* p38 α activation induced by the L16 switch with auto regulatory characteristics.

© 2006 Elsevier Ltd. All rights reserved.

Keywords: p38; mitogen activated protein kinase; active mutants; crystal structure; dimerization

*Corresponding author

Introduction

The p38 mitogen-activated protein (MAP) kinases are serine threonine kinases that are expressed in all eukaryotic cells and are activated in response to a variety of stimuli. Normal function of p38 is essential for both cellular and multicellular processes^{1,2} whereas abnormal p38 activity is associated with various diseases including chronic inflam-

matory diseases, psoriasis, myocardial-injuries and cancer.^{3,4} Accordingly, several studies indicate that p38 inhibitors could serve as therapeutic agents, particularly as anti-inflammatory drugs.⁵

There are four p38 isoforms (α , β , γ and δ) that belong to the MAP kinase superfamily which also includes the extracellular signal-regulated kinases (ERKs), the c-Jun N-terminal kinases (JNKs/SAPK) and the big MAP kinases (BMKs/ERK5 and ERK7).^{2,6} All MAP kinases share the same basic activation mechanism.⁷ They are characterized by a common activation motif composed of Thr-X-Tyr sequence located on a flexible loop termed the phosphorylation lip. In response to an appropriate stimulus the threonine and tyrosine in this motif are phosphorylated by dual specificity kinases termed MAP kinase kinases (MAPKKs or MKKs). This dual

Abbreviations used: MAP, mitogen-activated protein; MKK, MAP kinase kinase; ERK, extracellular signal-regulated kinase; β -OG, *n*-octyl- β -glucopyranoside; KD, kinase-dead.

E-mail address of the corresponding author:
oded.livnah@huji.ac.il

phosphorylation renders the enzymes catalytically active. Conversely, unphosphorylated MAP kinases exhibit no catalytic activity.^{8–10}

The MKK-mediated dual phosphorylation has been considered as the only path in which MAP kinases become active. Recently, two alternative mechanisms have been reported. The first involves p38 α interaction with TAB1, which promotes p38's autophosphorylation and self activation.¹¹ The second pathway, exclusive to T cells, involves phosphorylation of p38 α on Tyr323, a novel phosphorylation site, by ZAP-70 tyrosine kinase. Once phosphorylated on Tyr323, p38 α acquires autophosphorylation capabilities and subsequently becomes active.¹² Notably, both MKK-mediated p38 activation and the alternative pathways eventually result in phosphorylation of the phosphorylation lip.

The structural changes imposed by TAB1 or by phospho-Tyr323 that induce the autophosphorylation activity are not known. Crystal structures of Tyr323 phosphorylated p38 α or in complex with TAB1 are currently unavailable. The crystal structures of p38 α are available only in the inactive form^{13,14} and in a complex with various inhibitors and peptides (total of 41 structures). The only structure of an active form of p38 MAP kinase is the structure of the dually phosphorylated p38 γ .¹⁵ Detailed structural data regarding the difference between the active and inactive states of a MAP kinase is currently available only for ERK2.^{10,16}

The MAP kinase activation pathway is extremely intricate and interdigitated making the determination of the specific role of each MAP kinase a difficult task. Active p38 MAP kinases phosphorylate numerous substrates including other kinases, tumor suppressors and transcription and translation factors.² It is not known, however, if all downstream substrates are equally phosphorylated by all p38 isoforms. In fact, the physiological and/or pathological role of each p38 isoform or its splicing variants is not well understood. One of the useful means for addressing this question is the use of specific intrinsically active p38 mutants, which were long desired for but unavailable.

Recently we developed the first series of such intrinsically active molecules of p38 α and p38 γ ¹⁷ and subsequently of p38 β and p38 δ (Avitzour *et al.* unpublished results). These molecules are spontaneously active both *in vitro* (as purified recombinant proteins) and *in vivo* (in cell cultures; Askari *et al.* unpublished results). Two of the active mutants, p38 α ^{D176A + F327L} and p38 α ^{D176A + F327S} exhibited intrinsic activity *in vitro* that reached ~25% in reference to the dually phosphorylated p38 α ^{wt}.¹⁷

As these mutants are in a constant active state and maintain all biochemical and pharmacological properties of active p38,¹⁷ they can serve as a powerful tool for studying p38 biology as well as the structural basis for its activation and catalysis. Based on available structural data of inactive p38 α , we have identified three aromatic residues in the N' lobe, Tyr69, Phe327 and Trp337, that form a hydrophobic core which stabilizes the conformation of the L16

loop.¹⁷ A mutation in each of these three residues was found to activate p38 α or HOG1.^{17,18} We previously hypothesized that the L16 loop, normally stabilized by the hydrophobic core, is a natural element maintaining the low basal activity of p38. Moreover, we suggested that the conformation of L16 loop in the p38 α ^{wt} maintains its basal activity and conformational changes in this region could result in activation.¹⁷ This notion was supported by the fact that L16 loop conformation of both p38 γ ¹⁵ and ERK2^{10,16} is altered upon activation.

Here we present the crystal structures, at relatively high resolution, of three of the intrinsically active p38 α mutants.¹⁷ These structures reveal that mutations in the L16 loop region induce local conformational change that triggers protein activation. We further present biochemical data showing that the activation mechanism of the active mutants involves dimer formation, which leads to autophosphorylation activity that occurs *in trans*. p38 α ^{wt} molecules can participate in the formation of heterodimer with an active p38 molecule in which p38 α ^{wt} functions as a dominant negative molecule for autophosphorylation. These data explain the mechanism of activation of the intrinsically active mutants and also the mechanism used by the alternative activation pathways. The results further provide the first indications for functional dimerization of p38 α , and for the role of the L16 loop conformation in p38 activation.

Results and Discussion

The p38 α mutants are self-activated

The structural basis of p38 activation is not well understood. The intrinsically active p38 α mutants we recently developed¹⁷ allowed us to address this question. We therefore initiated an effort for obtaining crystals of our mutated active proteins. From numerous conditions assayed, crystals were reproducibly obtained only when proteins were purified from *Escherichia coli* cells grown at relatively low temperature (21 °C). We found, however, that these proteins were not catalytically active as compared to the corresponding p38 α proteins produced from cultures grown at 32 °C (Figure 1(a)). Comparison of the p38 α proteins purified from cultures grown at 21 °C and 32 °C revealed that they differ in their phosphorylation state (Figure 1(b)). The p38 α ^{wt} molecules were not phosphorylated when purified from an *E. coli* culture grown at either 21 °C or 32 °C (Figure 1(b)). On the other hand, active p38 α mutants purified from the 32 °C cultures were exclusively phosphorylated on threonine residues, and did not contain any phosphotyrosine (Figure 1(b)). We concluded that when expressed in *E. coli* cells grown at 32 °C, the intrinsically active p38 α variants are phosphorylated on Thr180, probably as a result of autophosphorylation activity.¹⁸ This notion suggests that the p38 α variants expressed in 21 °C are not phosphorylated but possess the

capability of autophosphorylation and autoactivation. To ratify this notion we tested the autophosphorylation capability of p38 $\alpha^{D176A+F327L}$ *in vitro* using the same protein batch used for crystallization (Figure 1(c)). We found that p38 $\alpha^{D176A+F327L}$ exhibited autophosphorylation capabilities whereas p38 α^{wt} did not (not shown). Given that p38 MAP kinases are serine/threonine kinases, it is not surprising that the autophosphorylation occurs

exclusively on threonine residues. The mono-phosphorylated form is both catalytically and biologically active as shown in the supporting information. In summary, the p38 α variants that were crystallized are not phosphorylated yet having intrinsic autophosphorylation capabilities.

Tyrosine phosphorylation is not essential for p38 α activity

In order to distinguish between the mono and the dually phosphorylated forms of p38 α we must use specific anti-phospho-tyrosine and anti-phospho-threonine. The fact that Thr-only phosphorylated molecules react with the anti-phospho-p38 antibody (Santa Cruz Biotechnology) is likely to occur as it was already shown that antibodies recognizing dually phosphorylated MAP kinases also interact with the Thr-only phosphorylated forms.^{19,20}

Mono-phosphorylated Hog1 on threonine was shown to be biologically active¹⁹ and the Tyr323-phosphorylated p38 α^{Y182F} mutant exhibited some catalytic activity.¹² To test whether mono-phosphorylated p38 α could also induce catalysis, we used active MKK6 to phosphorylate p38 α mutants *in vitro* lacking either Tyr182 or Thr180 phospho-acceptors. We found that the p38 α^{Y182F} mutant was catalytically active (~20% of maximum) after MKK6 phosphorylation, whereas phosphorylated p38 α^{T180A} molecules did not show any activity (Figure 1(d)).

These results show that phosphorylation solely on Thr180 is sufficient for p38 catalytic activity and

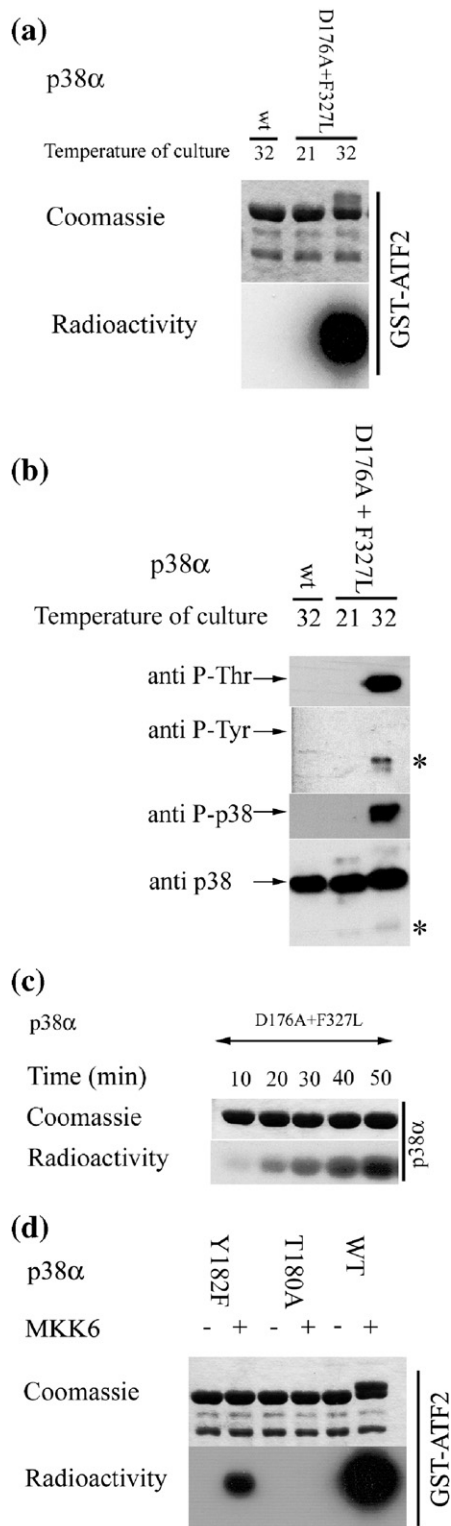


Figure 1. Phosphorylation on Thr180 of recombinant p38 $\alpha^{D176A+F327L}$ is temperature-dependent. (a) Kinase assay of p38 α^{wt} and p38 $\alpha^{D176A+F327L}$ purified from cultures grown at different temperatures. The assay measures the ability of the enzymes to phosphorylate *in vitro* the GST-ATF2 protein substrate using [γ -³²P]ATP. Coomassie staining (upper image) verified the amount of substrate in each lane. The radiograph (lower image) reveals the activity. (b) The active p38 α variant is threonine phosphorylated. To elucidate phosphorylation we preformed Western blot analysis utilizing specific anti-phospho antibodies (anti-phospho-Thr, anti-phospho-Tyr and anti-phospho-p38). The small arrows indicate the migration height of p38 α in gel electrophoresis. Anti-p38 α antibody was used to determine the amount of p38 loaded at each lane. Some minor phosphorylation on tyrosine residues can be seen only on smaller proteolytic products (marked with asterisks). Yet, these proteins also interacted with the anti-phospho-p38 antibody. (c) The p38 $\alpha^{D176A+F327L}$ molecule exhibits autophosphorylation *in vitro*. Purified p38 $\alpha^{D176A+F327L}$ that was also used for crystallization was incubated in a kinase assay buffer without substrate for increasing time intervals at 30 °C. Coomassie staining (upper image) verified the amount of enzyme in each lane. The radiograph (lower image) reveals phosphorylation. (d) Mono-phosphorylated p38 α is catalytically active. We measured kinase activity toward GST-ATF2 of p38 α^{Y182F} , p38 α^{T180A} and p38 α^{wt} activated or not *in vitro* by MKK6. Coomassie staining (upper image) verified the amount of GST-ATF2 in each lane. The radiograph (lower image) indicates activity.

support the idea that the active mutants acquire intrinsic activity through autophosphorylation of Thr180. Strikingly, the activity of the intrinsically active mutants (25% of maximum¹⁷) resembles the activity level manifested by the mono-phosphorylated p38 α ^{Y182F} mutant. The activity of these active mutants could be further enhanced by phosphorylation with MKK6,¹⁷ most probably as a result of the phosphorylation of Tyr182. Previous data are further supporting this notion as active mutants of Hog1 carrying the tyrosine to phenylalanine mutation maintained their intrinsic activity, but lost the ability to be further activated by their upstream activator.¹⁹ Thus, phosphorylation on threonine alone is sufficient for catalytic activity and additional phosphorylation on the tyrosine results in enhanced activity.

Overall structures

We have determined the structures of p38 α ^{D176A}, p38 α ^{D176A + F327S} and p38 α ^{D176A + F327L} to the highest resolutions to date (Table 1). The p38 α ^{D176A + F327S} crystallized in two forms using identical crystallization conditions (same experiment) with somewhat different cell parameters although maintaining the same space group. We have solved the structures

for both crystal forms (form-A and form-B). The cell dimensions of form-A are identical to those of the other two mutants whereas the 'b' axis of form-B is somewhat longer (Table 1). The structural differences between the two forms are negligible and we henceforth refer to p38 α ^{D176A + F327S} in form-A (unless specified otherwise). The structures of the p38 α mutants maintain the overall MAP kinase topology consisting of N' and the C' lobes forming the catalytic groove between them. Comparison of the mutant structures to p38 α ^{wt} (PDB code 1P38¹³) reveals a slight difference in the arrangement between the N' and the C' lobes (Figure 2(a)). In addition, the structures contain local conformational changes located in the vicinity of the mutations (Figures 2(a) and (b)).

The structures of all p38 α mutants contain three molecules of the detergent *n*-octyl- β -glucopyranoside (β -OG) that was a component of the crystallization solution (Figure 2(b)). One β -OG molecule (site 1; Figure 2(b)) was well defined and modeled in all crystal structures. Electron density maps indicated the presence and position of the other two β -OG molecules (sites 2 and 3) yet being pronounced and thus modeled only for p38 α ^{D176A + F327L}. The binding of the β -OG molecule in site 1 changes

Table 1. Data collection and refinement statistics

	p38 α ^{D176A + F327L}	p38 α ^{D176A}	p38 α ^{D176A + F327S} form-A	p38 α ^{D176A + F327S} form-B
ESRF beamline	ID14-4	ID14-3	ID29	ID29
Wavelength (Å)	0.925	0.931	0.953	0.979
Space group	<i>P</i> 2 ₁ 2 ₁ 2 ₁			
Unit cell parameters (Å)	<i>a</i> = 68.67 <i>b</i> = 69.79 <i>c</i> = 74.22	<i>a</i> = 67.86 <i>b</i> = 69.42 <i>c</i> = 74.06	<i>a</i> = 68.00 <i>b</i> = 69.68 <i>c</i> = 74.49	<i>a</i> = 68.93 <i>b</i> = 74.59 <i>c</i> = 74.13
Resolution range (Å)	40–1.45	50–1.83	48.8–1.70	31.2–1.86
Unique reflections	63,600	29,662	39,403	32,410
Redundancy	7.8	5.0	14.1	5.3
$R_{\text{sym}}(I)^a$	5.5 (66.8) ^b	8.8 (39.1) ^b	7.2 (44.2) ^b	5.7 (66.8) ^b
Completeness	99.4 (100.0) ^b	99.1 (95.3) ^b	99.7 (98.2) ^b	99.1 (99.9) ^b
I/σ	46.1 (3.1) ^b	22.0 (1.9) ^b	75.9 (5.8) ^b	45.8 (3.0) ^b
Number of protein atoms	2628	2628	2670	2638
Number of β -OG atoms	60	20	20	20
Number of solvent atoms	435	460	207	198
<i>R</i> -factor	20.6	17.5	21.9	22.3
<i>R</i> -free ^c	24.1	22.4	24.0	27.7
< <i>B</i> > (Å ²)				
Protein	27.4	22.1	36.4	42.9
β -OG	53.0 (29.2, 65.2, 64.5) ^d	24.1	37.9	46.6
Solvent	40.0	36.8	43.9	48.3
<i>RMSD from ideality</i>				
Bond length (Å)	0.010	0.017	0.017	0.017
Bond angle (°)	1.42	1.60	1.56	1.57
<i>Ramachandran plot (PROCHECK)</i>				
Favored (%)	93.8	91.3	89.2	90.1
Allowed (%)	6.2	8.3	9.8	8.6
Generously allowed (%)	0	0.3	1.0	1.4
Disallowed (%)	0	0	0	0

^a $R_{\text{sym}}(I) = \sum |I - \langle I \rangle| / \sum I$.

^b Outer shell resolution range 1.5–1.45 Å, 1.86–1.83 Å, 1.76–1.70 Å and 1.92–1.85 Å for p38 α ^{D176A + F327L}, p38 α ^{D176A}, p38 α ^{D176A + F327S} form-1 and p38 α ^{D176A + F327S} form-2, respectively.

^c Test set is 5% for all data.

^d Average temperature factors for β -OG molecules 1,2 and 3, respectively.

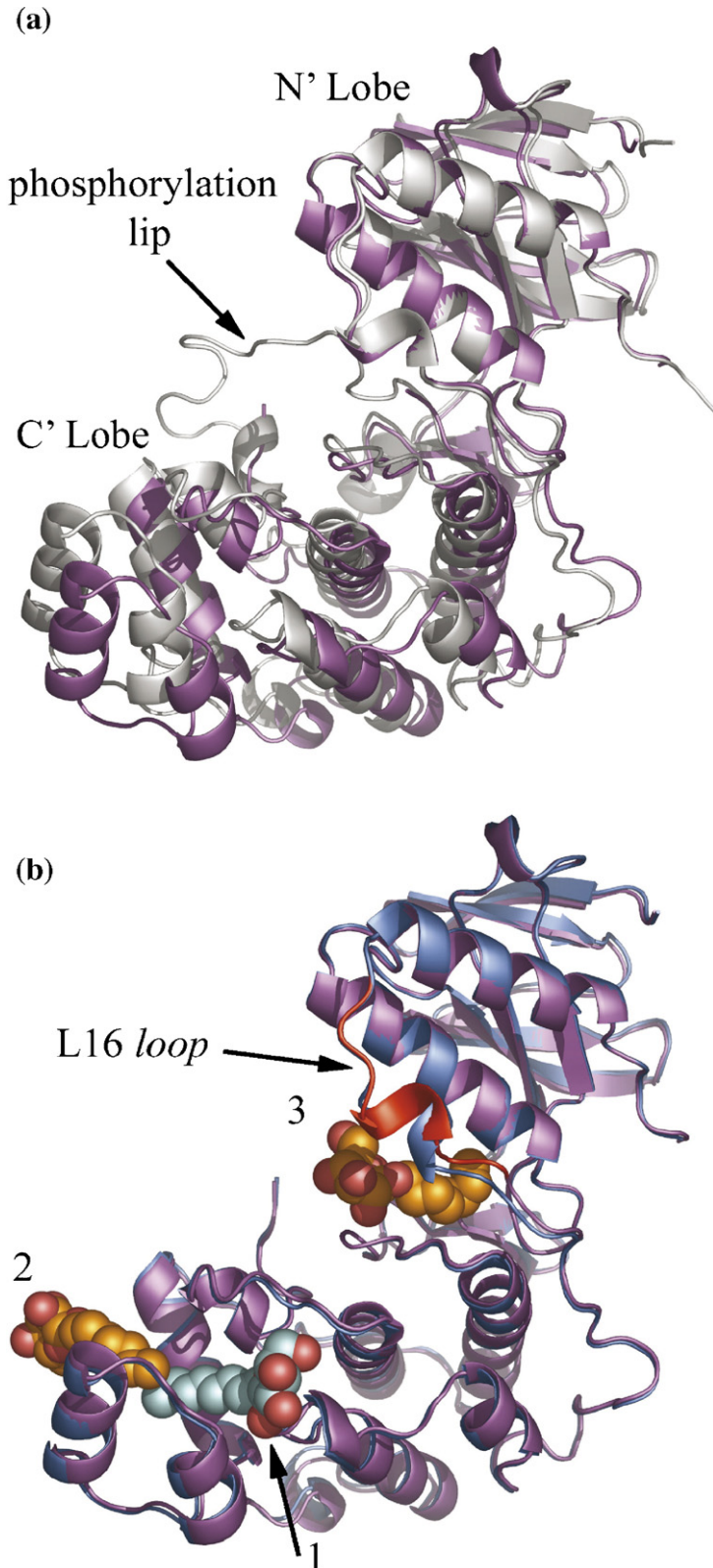


Figure 2. Overall structure. (a) Structural alignment of p38 α^{D176A} (magenta) and p38 α^{wt} (gray) by superimposing the kinase N' lobe. An arrow indicates the phosphorylation lip in the wild-type model. In the p38 α^{D176A} model and other mutants the loop is partially disordered lacking 14–15 residues. All molecular graphics in this work were rendered using PyMol [<http://pymol.sourceforge.net/>]. The general kinase topology is maintained although a small change in the orientation between the lobes is apparent. (b) Ribbon presentation of the superimposed structures of p38 $\alpha^{D176A+F327L}$ (blue) and p38 α^{D176A} (magenta) (omitting p38 $\alpha^{D176A+F327S}$ for clarity). The L16 loop, which goes through a conformational change, is shown in red. The three β -OG molecules are indicated by numbers and represented by spheres. β -OG molecules numbered 2 and 3 (orange) are exclusively included in the p38 $\alpha^{D176A+F327L}$ model whereas β -OG number 1 (cyan) is modeled in all the mutant structures.

the conformation of the “MAP kinase insertion” as well as the conformation of residues from the α EF/ α F loop as compared to the structure of p38 α^{wt} . These local conformational changes, however, are localized at the C' lobe away from the mutation sites and bare no significance to the structural analysis of the activation mutations.

Structural alterations that promote activation

Following the analysis of the overall structures, we examined the sites that upon mutations render p38 active: Phe327 in L16 loop, and Asp176 at the phosphorylation lip. Each of the mutations is sufficient to induce activation yet, when combined

a synergistic effect occurs.¹⁷ The phosphorylation lip (residues 171–183) of p38 α is a highly flexible loop. In this regard, most of the available crystal structures of p38 α are characterized by a high degree of disorder in the phosphorylation lip. This is a general phenomenon that is frequently observed in numerous structures of other protein kinases.²¹ As a result Asp176 is not modeled in any of the p38 α ^{wt} structures reported so far, nor is Ala176 in the crystal structures of the mutants. It implies that the replacement of a charged side-chain with a short methyl group, maintains the lip's flexibility, thus limiting the ability to interpret the exact structural role of the D176A mutation. We are addressing the possible effect of this mutation in view of additional biochemical results, as described below.

Replacement of Phe327 from the L16 loop (Figure 2(b)) to either serine or leucine renders the kinase intrinsically active (10% of maximum).¹⁷ All the residues of the L16 loop region are clearly defined in the electron density maps of all the mutant structures. The L16 loops of p38 α ^{D176A + F327L} and p38 α ^{D176A + F327S} adopt different conformations in which the residues that replaced Phe327 do not participate in stabilizing the hydrophobic core with Tyr69 and Trp337 (Figure 3(a)). The conformation of the L16 loop region in the structure of p38 α ^{D176A} is virtually identical to that of p38 α ^{wt}, confirming that the differences in the L16 loop in p38 α ^{D176A + F327L} and p38 α ^{D176A + F327S} are solely induced by the mutations in this region and not by other factors (Figure 3(b)). Since p38 α ^{D176A} possesses significant intrinsic activity by itself, the structural alterations of the L16 loop are not the only mechanism that promotes the mutants' activation. We assume, however, that mutating either Asp176 or Phe327 promotes autophosphorylation activity in a similar manner (discussed further below). The structures of the active mutants strongly support our initial hypothesis that disruption of the hydrophobic core promotes p38 α activation.¹⁷

Since two chemically contrasting alternations of Phe327, to either serine or leucine, are equally capable of activating p38 α , it seems that the activation results from a common conformational change in this region and not from the alteration *per se*. Thus, we have thoroughly analyzed the common conformational changes occurring in both p38 α ^{D176A + F327L} and p38 α ^{D176A + F327S} in comparison to p38 α ^{wt}. The two mutations in residue 327 result in a conformational change and a general shift of 1–1.5 Å of residues 323 to 329, relative to the non-active p38 α ^{wt} conformation. In the structure of the non-active p38 α ^{wt}, residues 325 to 330 adopt a 3_{10} -helix conformation. The mutations in Phe327 result in partial unwinding and shortening of this 3_{10} -helix helical segment. In the structure of p38 α ^{D176A + F327L} the helix consists of residues Asp324 to Glu328 and in p38 α ^{D176A + F327S} of only residues Ser326 to Ser329 (Figure 3(b)). The two mutants exhibit somewhat different conformations in the L16 loop region, which probably represent a subset of L16 conformations that promote autophosphorylation.

The conformational changes within the L16 loop segment reveal several intriguing aspects. Glu328 from the L16 loops of p38 α ^{wt} and p38 α ^{D176A} forms a salt-bridge interaction with Arg70 (Figure 3(c)). Due to the conformational changes in the L16 region this salt-bridge is disrupted in both structures of p38 α ^{D176A + F327L} and p38 α ^{D176A + F327S} (Figure 3(c)), although Glu328 adopts a different conformation in each mutant. The salt-bridge counterpart residue Arg70, that is conserved in all MAP kinases, interacts with the phosphorylated threonine upon activation, as seen in the phosphorylated structure of p38 γ .¹⁵ In the p38 family, Glu328 is a chemically conserved, negatively charged residue (substituted by Asp331 in p38 γ). In this respect, Asp331 of activated p38 γ is located in a short disordered segment, therefore not forming a salt-bridge interaction with the arginine from the C helix. Thus, the absence of this salt-bridge seems to be a characteristic of active conformation of p38s.

Are these structural changes also occurring when p38 α is activated through natural mechanisms? Salvador *et al.* have recently shown that in T cells p38 α activation is obtained *via* phosphorylation of Tyr323 that consequently induces autophosphorylation.¹² In the p38 α ^{wt} structure, Tyr323 is located in the L16 loop (Figure 3(b)) and its side-chain is directed into a hydrophobic patch and unavailable to solvent. Plausibly, upon phosphorylation the charged phospho-Tyr323 is repelled from the hydrophobic patch and becomes available to solvent followed by a conformational change in the L16 loop. These changes could be similar to those observed in residues 324 – 326 of p38 α ^{D176A + F327L} and p38 α ^{D176A + F327S}, which similarly to Tyr323-phosphorylated p38 α , acquired an autophosphorylation capability (Figure 1(c)). We thus postulate that the mutations in Phe327, to some degree, emulate the conformational changes that occur naturally when Tyr323 becomes phosphorylated. In this context, one may assume that a subset of allowed conformations in the L16 loop permit autophosphorylation and activation.

The L16 loop also appears to play a regulatory role that relates to protein activation in other MAP kinases. ERK2¹⁰ and p38 γ ¹⁵ are the only available structures of dually phosphorylated active MAP kinase. In addition, only ERK2 provides a definite comparison tool for activation induced changes, since the structure of its unphosphorylated inactive form is also available.¹⁶ In this context, several conformational changes occur in ERK2 upon activation, which include lobe closure and reorientation of the phosphorylation lip. In addition, the L16 loop goes through a notable conformational change, which results in the exposure of several leucine residues to solvent. In this regard, these leucine residues are an essential component in forming the dimer interface in the active state.^{10,25} For the p38 γ , an inactive structure is unavailable and therefore could only be compared to p38 α , which shares 63% sequence identity. In the native p38 α ^{wt} the L16 loop is well defined and ordered (Figure 3(a)) whereas in

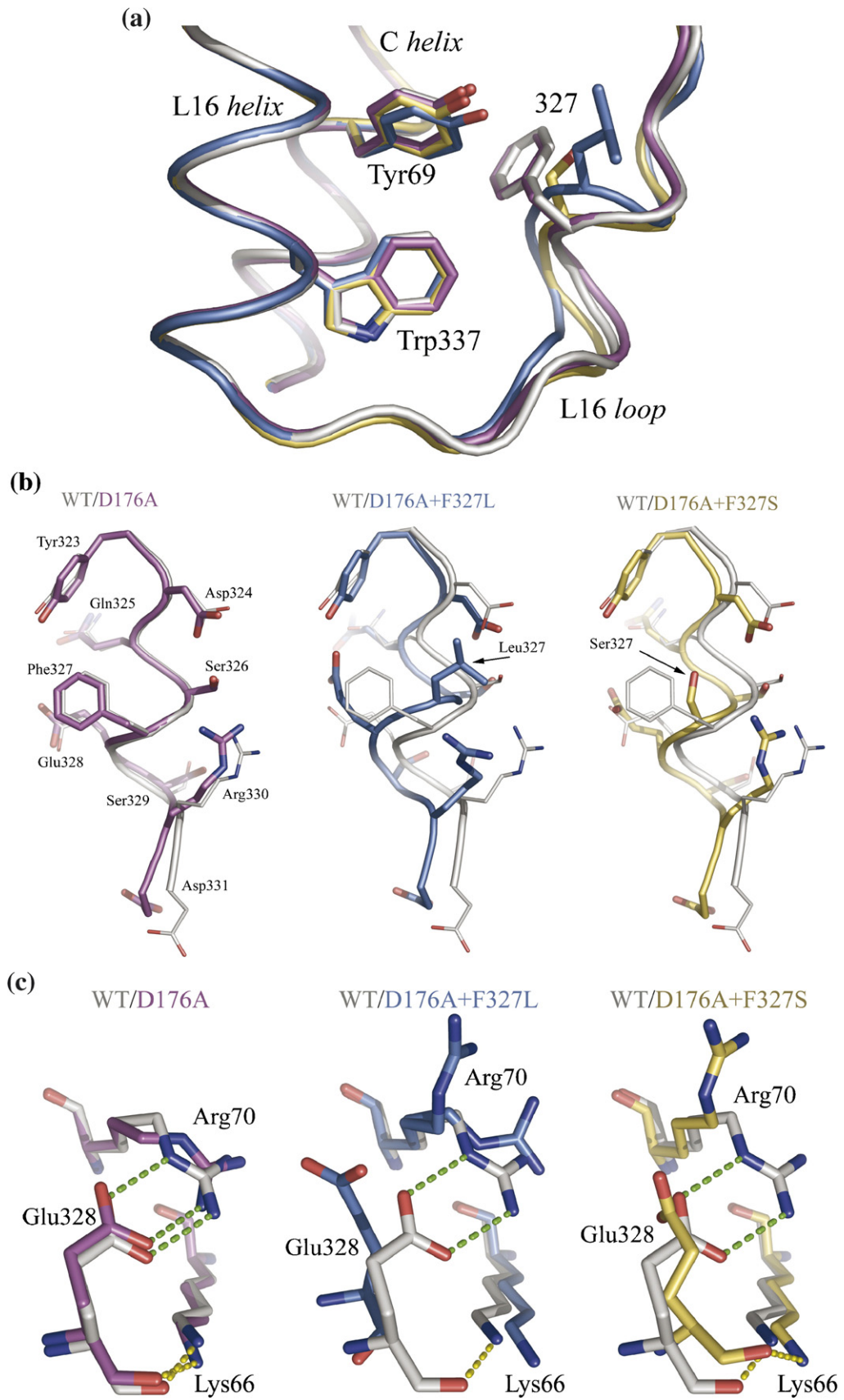


Figure 3 (legend on opposite page)

p38 γ it is partially disordered (five residues). For the JNK subfamily only the structures of unphosphorylated JNK1²² and JNK3²³ are available. In the absence of activated counterparts it is difficult to analyze the conformational changes upon activation. However, the L16 loop in these structures is completely disordered, indicating its flexibility and propensity to go through conformational changes upon activation. Taken together these results indicate that in MAP kinases the L16 region plays a fundamental role in the activation process. Upon activation, it was shown to go through conformational changes. Alternatively, as in our case, conformational changes induced by the mutations in this region can in turn mimic the active conformation and consequently induce activation.

p38 α 's autophosphorylation occurs *in trans* and involves dimerization

Having shown that the active mutants acquire their catalytic activity through autophosphorylation, we examined whether it occurs in *cis* or *trans*. We have mixed two different p38 molecules and monitored if they can phosphorylate each other. We first mixed p38 α^{wt} with either p38 α^{D176A} or p38 $\alpha^{D176A+F327L}$. The p38 α^{wt} protein in these mixtures contained a larger tag than the mutants, allowing separation and identification of the two molecules in gel electrophoresis. The p38 α^{wt} protein did not become phosphorylated when incubated with any of the mutants (Figure 4(a)). Surprisingly, the presence of p38 α^{wt} in solution inhibited the autophosphorylation capability of the mutants. This inhibition was found to be dose dependant (Figure 4(b)). In a stoichiometry ratio of approximately 1:1, the inhibition is almost complete. Thus, p38 α^{wt} acts as a dominant negative molecule in this assay, preventing auto-activation of the mutants (note that the molecules used were from a culture grown at 21 °C), strongly indicates that p38 α^{wt} interacts with the active p38 α mutant molecules forming an inactive dimer. We thus conclude that the triggering of the autophosphorylation of the active mutants depended on mutual - *trans* interactions. It is plausible that the active p38 molecules interact in a

transient manner and at a lower affinity than with p38 α^{wt} . To further test this idea, we have created a series of "kinase-dead" (KD) variants of our p38 α proteins by introducing a K53A mutation. We have verified that the resulting molecules were catalytically inactive even after MKK6 phosphorylation (data not shown). We then mixed active p38 α molecules with their KD variants (i.e. p38 $\alpha^{D176A+F327L}$ and p38 $\alpha^{D176A+F327L+K53A}$) (Figure 4(c)). If dimerization occurs, this mixture should contain three types of dimers: active:active, KD:KD and active:KD (Figure 4(d)). If autophosphorylation occurs *in trans* then KD molecules in the latter dimer should be phosphorylated (one-third of all KD molecules present) as well as active molecules of the first dimer (2/3 of all active molecules present). As is shown in Figure 4(c), the p38 $\alpha^{D176A+F327L+K53A}$ (KD) was phosphorylated in the presence of p38 $\alpha^{D176A+F327L}$. The phosphorylation extent of the p38 $\alpha^{D176A+F327L+K53A}$ (KD) molecules was approximately half compared to that of p38 $\alpha^{D176A+F327L}$ as expected. We thus conclude that the autophosphorylation occurs *in trans* and depends on protein interaction (dimer formation) and on mutual-*trans* triggering (Figure 4(d)).

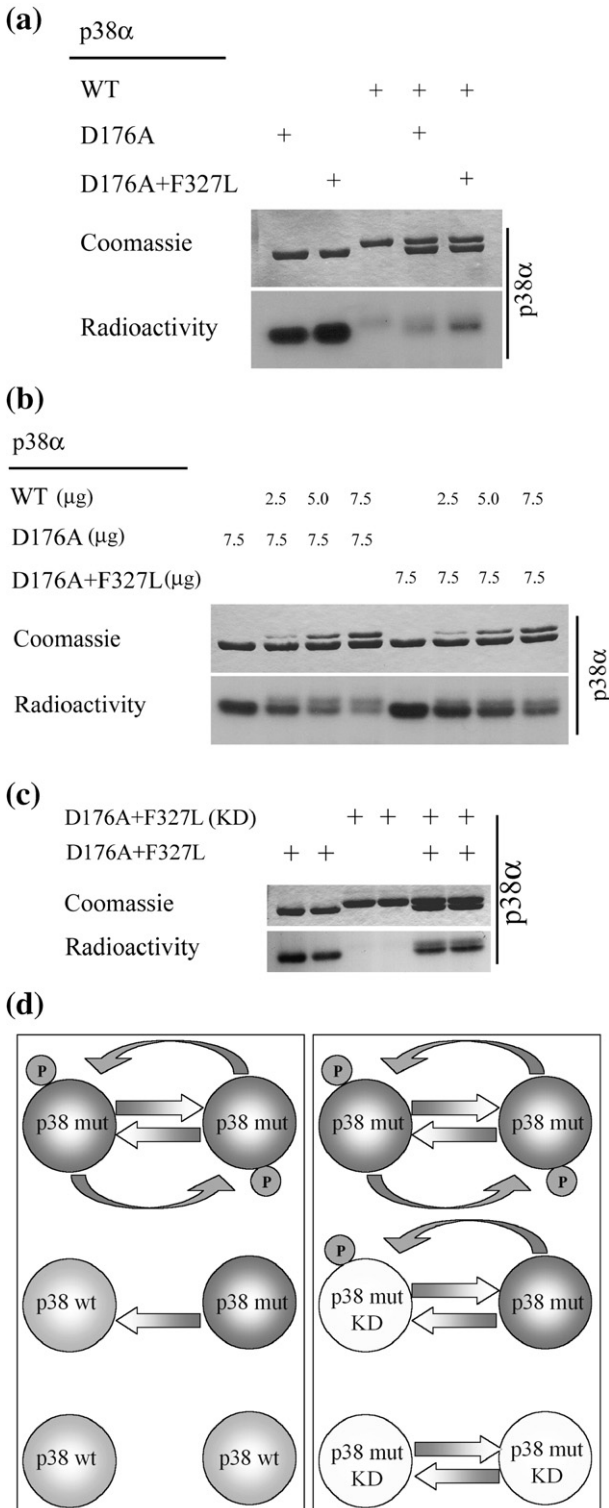
The finding that p38s dimerize raises the possibility that various dimers may form *in vivo*. These include an autophosphorylation-capable homodimer of two active p38 α molecules (Tyr323-phosphorylated or carrying the activating mutation), an inactive heterodimer composed of the p38 α^{active} :p38 α^{wt} complex and perhaps even an inactive p38 α^{wt} :p38 α^{wt} homodimer. Dimerization of p38 α , resulting from Tyr323 phosphorylation, was proposed previously.²⁴ The dominant negative effect of p38 α^{wt} suggests that combinatorial dimerization is a novel mode of regulation for p38. Namely, there may be an *in vivo* threshold for activating p38 α by autophosphorylation. A small fraction of Tyr323 phosphorylated p38 α molecules would be insufficient for activation, as these molecules will be inhibited by a higher concentration of the unphosphorylated p38 α . Since there must be a mutual influence of two mutants in order to promote autophosphorylation, we hypothesize that they interact in a symmetrically paired manner (identical residues from each monomer contribute to the

Figure 3. Conformational changes in the L16 loop and disruption of a salt-bridge are fingerprints of the active p38 α molecules. (a) The conformational changes within the L16 loops of p38 $\alpha^{D176A+F327L}$ (blue) and p38 $\alpha^{D176A+F327S}$ (yellow) in reference to p38 α^{D176A} (magenta) and p38 α^{wt} (gray). Mutations of Phe327 to serine or leucine results in a conformational change in the L16 loop. Residues 327 in the mutants' structures subsequently adopt a different conformation. However, the conformation of Trp337 and Tyr69 remains highly similar in all structures. (b) Segments of L16 loop from p38 α^{D176A} (left), p38 $\alpha^{D176A+F327L}$ (center) and p38 $\alpha^{D176A+F327S}$ (right) are superimposed with p38 α^{wt} as a reference. The conformation of the L16 loop in the structure of p38 α^{D176A} is almost identical (except minor changes in Asp331) to that of p38 α^{wt} . Mutation of Phe327 leads to the unwinding and a shift of the main-chain helical conformation in the L16, and subsequently the side-chains of residues 324 to 330 adopt a different position in both p38 $\alpha^{D176A+F327L}$ and p38 $\alpha^{D176A+F327S}$ models (center and right). (c) A salt bridge interaction is formed between the negatively charged carboxyl group of Glu328 and the positively charged guanidine of Arg70 (green broken lines) in both p38 α^{wt} and p38 α^{D176A} (left). This salt bridge is disrupted in the structures of p38 $\alpha^{D176A+F327L}$ and p38 $\alpha^{D176A+F327S}$ (center and right, respectively) due to the conformational change in the L16 loop. In this regard, the unpaired Arg70 acquire new conformations; in p38 $\alpha^{D176A+F327S}$ Arg70 adopts a dual conformation whereas in p38 $\alpha^{D176A+F327L}$ only one. The C α atom of Glu328 is shifted 2.53 Å and 1.11 Å in the structures of p38 $\alpha^{D176A+F327L}$ and p38 $\alpha^{D176A+F327S}$, respectively, relative to the p38 α^{wt} structure. The orientation of the side-chains is somewhat different as Lys66 is stabilizing the carbonyl oxygen of Glu328 by forming an H-bond interaction in p38 $\alpha^{D176A+F327S}$ similar to p38 α^{wt} but not in p38 $\alpha^{D176A+F327L}$ (yellow broken lines).

dimer formation) as proposed for ERK2 dimerization.²⁵ Furthermore, we assume that both the L16 loop and the Asp176 region participate in this dimer interface.

In summary, the structural basis of p38 α activation is not well understood. Here we have solved the crystal structures of three intrinsically active mutants of p38 α . These structures reveal that local conformational changes in the L16 loop promote autophosphorylation

on Thr180, which renders the enzyme catalytically active. These structures, however, did not disclose the structural consequences of mutating Asp176 on the phosphorylation lip. Nevertheless, mutating either or both residues on the L16 loop and the phosphorylation lip promote *trans*-autophosphorylation. The autophosphorylation is temperature dependent and involves dimer formation. Thus, the structural alterations in the L16 loop and the mutation of Asp176 on the phosphorylation lip promote, in different ways, the formation of an active dimer with autophosphorylation capabilities. When a p38 α^{wt} molecule is part of such a dimer, it functions as a dominant negative for the autophosphorylation activity. We have concluded that our mutations in the L16 loop region emulate mechanistically and structurally the activation of p38 α in T cells by phosphorylation of Tyr323.¹² Since the autophosphorylation is restricted to Thr180, the monophosphorylated p38 α may exhibit different substrate preferences and a physiological effect than those of dually phosphorylated p38 α .



Materials and Methods

Subcloning, expression, purification and analysis of p38 α active mutants

Polymerase chain reactions (PCR) were used to introduce six Histidine residues in-frame to the N' of p38 α (5' - AATAACCATGGCGCATCATCATCATCATCTCTCAG-GAGAGGCCACGTTCTACCG, 5' - ATGGATCCTCAG-GACTCCATCTCTTCTTGGTC). The PCR products where

Figure 4. p38 α^{wt} is dominant-negative for the *trans*-autophosphorylation activity. (a) Autophosphorylation is inhibited by p38 α^{wt} . We have performed a kinase assay reaction at 30 °C with the indicated p38 α proteins without a protein substrate and separated the reaction mixture using SDS-PAGE. The reactions were performed in equal volumes and the same amount of solution was loaded in each lane. Coomassie staining (upper images) indicates the protein's concentrations, the radiograph (lower images) reveals autophosphorylation. The molecular mass of p38 α^{wt} is slightly heavier because of a longer tag as compared to the mutants (upper band). (b) The autophosphorylation inhibition characterizes with a dose response. We repeated the experiment as described for (a), except using varied amounts of p38 α^{wt} in the reactions. (c) The autophosphorylation occur *in trans*. We performed a similar experiment with a kinase-dead (KD) p38 $\alpha^{D176A+F327L}$ mutant (upper band) and a short p38 $\alpha^{D176A+F327L}$. (d) Schematic representation of the various possible dimer formations in the first and second autophosphorylation experiment (left and right boxes, respectively). The triggering effect is represented by straight arrows and the phosphorylation activity by curved arrows. The inhibitory effect of p38 α^{wt} is demonstrated in the middle pair (left). On the one hand p38 α^{wt} cannot trigger the phosphorylation activity of p38 α^{mut} , on the other hand it prevents it from interacting with other p38 α^{mut} molecules to form an active dimer. As apposed to p38 α^{wt} , the p38 α^{mut} (KD) can trigger the *trans*-phosphorylation activity (right) of a regular p38 α^{mut} but cannot reciprocally phosphorylate the counterpart, thus a 1:2 labeling ratio is obtained.

digested with NcoI and BamHI and ligated to NcoI/BamHI digested pET-28a (Novagen). The vector plasmids containing the p38 α genes were introduced into Rosseta™ strain of *E. coli* (Novagen). An over-night 25 ml starter culture was inoculated into 1.5l of fresh Luria-Broth (LB) medium containing ampicillin/chloramphenicol and grown at 37 °C to $A_{600}=0.4$ and then transferred to 21 °C for 30 min. Protein expression was obtained by supplementing the media with 0.2 mM of Isopropyl- β -D-thiogalactopyranoside (IPTG) for 5 h. The cells were collected by centrifugation and stored at -20 °C. For lysis the cell pellets were thawed on ice and suspended in buffer A containing: 0.5 M NaCl, 50 mM Tris-HCl buffer (pH 7.4), 10 mM Imidazole supplemented with proteases inhibitors cocktail (Sigma) and disrupted mechanically using micro-fluidizer (model M-110 EHIS; Microfluidics Corp., Newton MA). The soluble and insoluble phases were separated by centrifugation (40,000g for 50 min). The supernatant was loaded on a buffer A pre-equilibrated Ni²⁺-chelating Sepharose column (Amersham), extensively washed and eluted using a linear gradient of imidazole in buffer A. The protein-containing fractions were pooled, dialyzed against 100 mM NaCl, 25 mM Tris-HCl (pH 7.4), 1 mM EDTA and were further dialyzed against 100 mM NaCl, 25 mM Tris-HCl (pH 7.4), 10 mM MgCl₂, 1 mM DTT. Consequently, the protein was loaded on a source 15Q anion exchange column (Amersham) equilibrated with 100 mM NaCl, 50 mM Tris-HCl (pH 7.4), 5% (v/v) glycerol, 10 mM MgCl₂, 1 mM DTT and then eluted using a linear gradient of NaCl in the same buffer. Purified protein was diluted 1:1 with 10 mM DTT, 10 mM MgCl₂, 5% glycerol and concentrated using Vivaspin™ (VivaScience) up to 14 mg/ml (determined by absorption at 280 nm) and stored at -80 °C. Kinase assay was performed as described.¹⁷ Autophosphorylation experiments were performed in similar reaction conditions as the kinase assay with few exceptions. These reactions were performed without adding the GST-ATF2 protein substrate, in a total volume of 20 μ l, with a higher enzyme concentration (4 mg/ml or as indicated in the relevant Figure) and using longer reaction times as indicated in the relevant Figure legends (up to 100 min).

Crystallization

Crystals for all mutants were obtained using the sitting-drop vapor diffusion method at 20 °C with the reservoir solution containing 10%–15% (w/v) PEG 3350, 100 mM Hepes (pH 7.25), 200 mM KF, 25 mM β -OG. The thin plate-shaped crystals reached their final size within two to three days but were unsuitable for crystallographic analysis. Crystals were further enlarged by streak seeding²⁶ and subsequent incubation at 4 °C to the size of 0.3 mm \times 0.3 mm \times 1.0 mm within seven to nine days. All mutants' crystals were cryo-protected in Paratone-N oil and immediately flash cooled to 100K for diffraction data collection.

Crystallographic data collection and refinement

Crystallographic data for the p38 α ^{D176A + F327L} were collected at the European Synchrotron Radiation Facility (ESRF) beamline ID14-4 ($\lambda=0.925$ Å) on an ADSC Quantum 4R CCD detector with the oscillation range of 0.5°. Data for p38 α ^{D176A} were collected at ESRF on beamline ID14-3 ($\lambda=0.931$ Å) on an MAR 165 CCD detector with the oscillation range of 0.5°. Data for p38 α ^{D176A + F327S} were collected at ESRF on beamline ID29 ($\lambda=0.953$ Å) on an ADSC Quantum 315 CCD

detector with the oscillation range of 0.5°. Data for all crystals were integrated and scaled using the HKL suite.²⁷ The crystals of the three p38 α mutants belonged to the orthorhombic $P2_12_12_1$ space group, with one molecule in the asymmetric unit (Table 1).

The structure of p38 α ^{D176A + F327L} was solved *via* molecular replacement methods using MOLREP²⁸ implemented in CCP4i using the atomic coordinates of p38 (1WFC)¹⁴ as search model after removing all solvent molecules. The solution resulted in an R_{factor} of 0.48 and correlation coefficient (CC) of 0.45 in the resolution range of 40 Å–4.0 Å. The initial $F_{\text{obs}}-F_{\text{calc}}$ and $2F_{\text{obs}}-F_{\text{calc}}$ electron density maps calculated after the five cycles of restrained refinement using REFMAC5²⁹ indicated conformational changes in the mutated region of L16. The structure was further refined in the resolution range of 40 Å–1.45 Å using REFMAC5 and solvent molecules were added utilizing ARP/wARP.³⁰ The structure was fitted into electron density maps using the graphics program O.³¹ The final model of p38 α ^{D176A + F327L} ($R_{\text{factor}}=20.6$; $R_{\text{free}}=24.1$) consists of residues 5–31, 36–114, 120–168, and 184–352, with 435 solvent and three β -OG molecules (Table 1).

The space group and unit cell parameters of the p38 α ^{D176A} mutant were virtually identical to those of the p38 α ^{D176A + F327L} and thus the structure was initially refined using the rigid-body protocol in REFMAC5.²⁹ The structure was further refined using REFMAC5 and solvent molecules were added with ARP/wARP³⁰ in a similar protocol described above. The model of p38 α ^{D176A} ($R_{\text{factor}}=17.5$; $R_{\text{free}}=22.4$) consists of residues 5–31, 36–114, 119–168, and 184–353, with 460 solvent and one β -OG molecule (Table 1).

Two crystal forms of p38 α ^{D176A + F327S}, distinct by the cell parameters along the b axis were analyzed. The structures were solved by the molecular replacement method using MOLREP²⁸ using the refined structure of p38 α ^{D176A + F327L} as the search model. The structures were further refined using REFMAC5 and solvent molecules were added by ARP/wARP³⁰ in a similar protocol as described above for the p38 α ^{D176A + F327L}. The model of p38 α ^{D176A + F327S} form-A ($R_{\text{factor}}=0.219$; $R_{\text{free}}=0.240$) consists of residues 4–34, 36–115, 120–168, and 183–354, with 207 solvent and one β -OG molecule (Table 1). The model of p38 α ^{D176A + F327S} form-B ($R_{\text{factor}}=22.3$; $R_{\text{free}}=27.7$) consists of residues 4–31, 36–115, 121–169, and 184–352, with 198 solvent and one β -OG molecule (Table 1).

Protein Data Bank accession codes

The atomic coordinates have been deposited and are available at the RCSB Protein Data Bank³² with accession codes 2FST for p38 α ^{D176A + F327L}, 2FSO for p38 α ^{D176A}, 2FSL for p38 α ^{D176A + F327S} form-A, and 2FSM for p38 α ^{D176A + F327S} form-B.

Acknowledgements

This work was supported by Israeli Science Foundation (ISF) grants 495-03 (to O. L.) and funds from the Altertum Elsa and Elyahu Pen Foundations (to O. L. and D. E.). We thank Mr Nadav Askari for providing p38 α ^{Y182F} and p38 α ^{T180A} mutants. We thank the staff of the ESRF, Grenoble, France for their helpful assistance.

References

- Zarubin, T. & Han, J. (2005). Activation and signaling of the p38 MAP kinase pathway. *Cell Res.* **15**, 11–18.
- Ono, K. & Han, J. (2000). The p38 signal transduction pathway: activation and function. *Cell Signal.* **12**, 1–13.
- Engelberg, D. (2004). Stress-activated protein kinases—tumor suppressors or tumor initiators? *Semin. Cancer Biol.* **14**, 271–282.
- Lee, J. C., Kumar, S., Griswold, D. E., Underwood, D. C., Votta, B. J. & Adams, J. L. (2000). Inhibition of p38 MAP kinase as a therapeutic strategy. *Immunopharmacology*, **47**, 185–201.
- Kumar, S., Boehm, J. & Lee, J. C. (2003). p38 MAP kinases: key signalling molecules as therapeutic targets for inflammatory diseases. *Nature Rev. Drug Discov.* **2**, 717–726.
- Cano, E. & Mahadevan, L. C. (1995). Parallel signal processing among mammalian MAPKs. *Trends Biochem. Sci.* **20**, 117–122.
- Songyang, Z., Lu, K. P., Kwon, Y. T., Tsai, L. H., Filhol, O., Cochet, C. *et al.* (1996). A structural basis for substrate specificities of protein Ser/Thr kinases: primary sequence preference of casein kinases I and II, NIMA, phosphorylase kinase, calmodulin-dependent kinase II, CDK5, and Erk1. *Mol. Cell. Biol.* **16**, 6486–6493.
- Robbins, D. J., Zhen, E., Owaki, H., Vanderbilt, C. A., Ebert, D., Geppert, T. D. & Cobb, M. H. (1993). Regulation and properties of extracellular signal-regulated protein kinases 1 and 2 in vitro. *J. Biol. Chem.* **268**, 5097–5106.
- Cobb, M. H. & Goldsmith, E. J. (2000). Dimerization in MAP-kinase signaling. *Trends Biochem. Sci.* **25**, 7–9.
- Canagarajah, B. J., Khokhlatchev, A., Cobb, M. H. & Goldsmith, E. J. (1997). Activation mechanism of the MAP kinase ERK2 by dual phosphorylation. *Cell*, **90**, 859–869.
- Ge, B., Gram, H., Di Padova, F., Huang, B., New, L., Ulevitch, R. J. *et al.* (2002). MAPKK-independent activation of p38 α mediated by TAB1-dependent autophosphorylation of p38 α . *Science*, **295**, 1291–1294.
- Salvador, J. M., Mittelstadt, P. R., Guszczynski, T., Copeland, T. D., Yamaguchi, H., Appella, E. *et al.* (2005). Alternative p38 activation pathway mediated by T cell receptor-proximal tyrosine kinases. *Nature Immunol.* **6**, 390–395.
- Wang, Z., Harkins, P. C., Ulevitch, R. J., Han, J., Cobb, M. H. & Goldsmith, E. J. (1997). The structure of mitogen-activated protein kinase p38 at 2.1-Å resolution. *Proc. Natl Acad. Sci. USA*, **94**, 2327–2332.
- Wilson, K. P., Fitzgibbon, M. J., Caron, P. R., Griffith, J. P., Chen, W., McCaffrey, P. G. *et al.* (1996). Crystal structure of p38 mitogen-activated protein kinase. *J. Biol. Chem.* **271**, 27696–27700.
- Bellon, S., Fitzgibbon, M. J., Fox, T., Hsiao, H. M. & Wilson, K. P. (1999). The structure of phosphorylated p38 γ is monomeric and reveals a conserved activation-loop conformation. *Structure*, **7**, 1057–1065.
- Zhang, F., Strand, A., Robbins, D., Cobb, M. H. & Goldsmith, E. J. (1994). Atomic structure of the MAP kinase ERK2 at 2.3 Å resolution. *Nature*, **367**, 704–711.
- Diskin, R., Askari, N., Capone, R., Engelberg, D. & Livnah, O. (2004). Active mutants of the human p38 α mitogen-activated protein kinase. *J. Biol. Chem.* **279**, 47040–47049.
- Bell, M., Capone, R., Pashtan, I., Levitzki, A. & Engelberg, D. (2001). Isolation of hyperactive mutants of the MAPK p38/Hog1 that are independent of MAPK kinase activation. *J. Biol. Chem.* **276**, 25351–25358.
- Bell, M. & Engelberg, D. (2003). Phosphorylation of Tyr-176 of the yeast MAPK Hog1/p38 is not vital for Hog1 biological activity. *J. Biol. Chem.* **278**, 14603–14606.
- Bardwell, L., Cook, J. G., Voora, D., Baggott, D. M., Martinez, A. R. & Thorner, J. (1998). Repression of yeast Ste12 transcription factor by direct binding of unphosphorylated Kss1 MAPK and its regulation by the Ste7 MEK. *Genes Dev.* **12**, 2887–2898.
- Nolen, B., Taylor, S. & Ghosh, G. (2004). Regulation of protein kinases; controlling activity through activation segment conformation. *Mol. Cell.* **15**, 661–675.
- Heo, Y. S., Kim, S. K., Seo, C. I., Kim, Y. K., Sung, B. J., Lee, H. S. *et al.* (2004). Structural basis for the selective inhibition of JNK1 by the scaffolding protein JIP1 and SP600125. *EMBO J.* **23**, 2185–2195.
- Xie, X., Gu, Y., Fox, T., Coll, J. T., Fleming, M. A., Markland, W. *et al.* (1998). Crystal structure of JNK3: a kinase implicated in neuronal apoptosis. *Structure*, **6**, 983–991.
- Mittelstadt, P. R., Salvador, J. M., Fornace, A. J., Jr & Ashwell, J. D. (2005). Activating p38 MAPK: new tricks for an old kinase. *Cell Cycle*, **4**, 1189–1192.
- Khokhlatchev, A. V., Canagarajah, B., Wilsbacher, J., Robinson, M., Atkinson, M., Goldsmith, E. & Cobb, M. H. (1998). Phosphorylation of the MAP kinase ERK2 promotes its homodimerization and nuclear translocation. *Cell*, **93**, 605–615.
- Stura, E. A. & Wilson, I. A. (1991). Application of the streak seeding technique in protein crystallization. *J. Cryst. Growth*, **110**, 270–282.
- Otwinowski, Z. & Minor, W. (1997). Processing of X-ray Diffraction Data Collected in Oscillation Mode. In *Methods in Enzymology*, vol. 276, pp. 307–326. Academic Press, New York.
- Vagin, A. A. & Isupov, M. N. (2001). Spherically averaged phased translation function and its application to the search for molecules and fragments in electron-density maps. *Acta Crystallog. sect. D*, **57**, 1451–1456.
- Murshudov, G. N., Vagin, A. A. & Dodson, E. J. (1997). Refinement of macromolecular structures by the maximum-likelihood method. *Acta Crystallog. sect. D*, **53**, 240–255.
- Morris, R. J., Perrakis, A. & Lamzin, V. S. (2003). ARP/wARP and automatic interpretation of protein electron density maps. *Methods Enzymol.* **374**, 229–244.
- Jones, T. A., Zou, J. Y. & Cowan, S. W. (1991). KJELDGAARD Improved methods for building protein models in electron density maps and the location of errors in these models. *Acta Crystallog. sect. A*, **47**, 110–119.
- Berman, H. M., Battistuz, T., Bhat, T. N., Bluhm, W. F., Bourne, P. E., Burkhardt, K. *et al.* (2002). The Protein Data Bank. *Acta Crystallog. sect. D*, **58**, 899–907.

Edited by I. Wilson

(Received 20 July 2006; received in revised form 7 August 2006; accepted 15 August 2006)
Available online 22 August 2006